Atmos. Chem. Phys., 8, 5669–5682, 2008
www.atmos-chem-phys.net/8/5669/2008/

Atmospheric Chemistry and Physics

Origin of diversity in falling snow

J. Nelson

College of Science and Engineering, Ritsumeikan University, Nojihigashi 1-1-1, Kusatsu 525-8577, Japan

Received: 20 December 2007 – Published in Atmos. Chem. Phys. Discuss.: 4 March 2008
Revised: 30 July 2008 – Accepted: 19 August 2008 – Published: 26 September 2008

Abstract. This paper presents a systematic way to examine the origin of variety in falling snow. First, we define shape diversity as the logarithm of the number of possible distinguishable crystal forms for a given resolution and set of conditions, and then we examine three sources of diversity. Two sources are the range of initial-crystal sizes and variations in the trajectory variables. For a given set of variables, diversity is estimated using a model of a crystal falling in an updraft. The third source is temperature-updraft heterogeneities along each trajectory. To examine this source, centimeter-scale data on cloud temperature and updraft speed are used to estimate the spatial frequency (m^{-1}) of crystal feature changes. For air-temperature heterogeneity, this frequency decays as $p^{-0.66}$, where p is a measure of the temperature-deviation size. For updraft-speed heterogeneity, the decay is $p^{-0.50}$. By using these frequencies, the fallpath needed per feature change is found to range from ∼0.8 m, for crystals near −15°C, to ∼8 m near −19°C – lengths much less than total fallpath lengths. As a result, the third source dominates the diversity, with updraft heterogeneity contributing more than temperature heterogeneity. Plotted against the crystal's initial temperature (−11 to −19°C), the diversity curve is "mitten shaped", having a broad peak near −15.4°C and a sharp subpeak at −14.4°C, both peaks arising from peaks in growth-rate sensitivity. The diversity is much less than previous estimates, yet large enough to explain observations. For example, of all snow crystals ever formed, those that began near −15°C are predicted to all appear unique to 1-μm resolution, but those that began near −11°C are not.

1 Introduction

The deposition of water vapor in air produces crystals with a surprising degree of variety, symmetry, and intricacy. Formation of various intricate features have been studied on-and-off over the years (e.g. Nakaya, 1954; Yamashita, 1976; Frank, 1982; Hallett and Knight, 1994; Nelson, 2005), and the symmetry is now understood to arise from the growth mode (Frank, 1982), but the sources of snow crystal variety have not been examined systematically.

The variety is generally equated to the number of possible crystal forms, a quantity that has been estimated through two approaches. The first approach is to estimate the number of possible distinct crystal forms for a given crystal radius (e.g. Knight and Knight, 1973). However, this approach yields no insights into the origin of the variety and it does not include limitations from the growth process; in particular, we neither learn the role of the crystal-growth response to the environment nor do we see how this response may limit the types of crystal forms. A different approach was suggested much earlier by Bentley (1901) when he wrote that the various crystal features originate from the various "atmospheric layers" the crystal falls through[1]. As a preliminary step in this direction, Hallett (1984) used knowledge of the crystal response to estimate the variety. His result, about $10^{30\,000}$, is immense (and much less than the $\sim 10^{3\,000\,000}$ of the first approach), but the method involved guessing the crystal's environment. Now, 34 years later, we still do not know if crystals pass through enough "layers" (regions) to produce the observed variety, or even if those layers are the main source of variety. We address these questions here, and suggest that the answer to both is "yes".

Correspondence to: J. Nelson
(jnelson@se.ritsumei.ac.jp)

[1]He earlier used the more poetic expression "Was ever life history written in more dainty hieroglyphics!" (1898). Some time later (∼1939), Nakaya expressed a similar idea in his now famous expression, translated as "A snow crystal is a letter from the sky".

Published by Copernicus Publications on behalf of the European Geosciences Union.

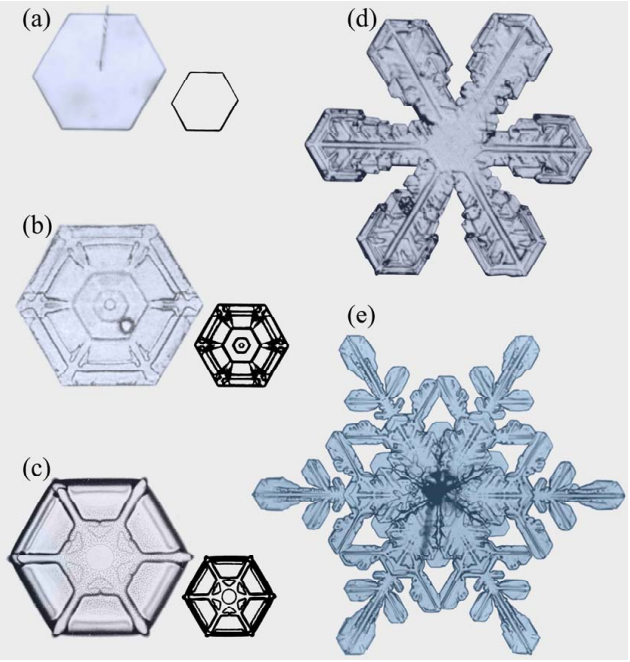

Fig. 1. Tabular snow crystals and their distinguishing features. Crystal **(a)** grew at low humidity near −9°C in constant conditions, suspended by a capillary (radial line). The perimeter shows the six prism faces. Crystal **(b)** grew in free-fall under nearly constant conditions of −12.2°C and liquid-water saturation (Takahashi et al., 1991). Crystals **(c)**–**(e)** are from natural snowfall. Distinguishing features of **(a)**–**(c)** are sketched, half-size, at right. Crystal **(e)** likely grew near −14°C. All crystals viewed in transmitted light. Photos **(b)**–**(e)** courtesy of Tsuneya Takahashi.

This paper described a growth-deviation model to systematically examine contributions to snow-crystal variety from several sources. These sources are the initial states of a crystal, idealized (constant updraft) trajectories to cloudbase, and modifications to the trajectories from temperature and updraft heterogeneities. By analyzing temperature and updraft-speed heterogeneities from recent cloud data, we derive an air-region thickness corresponding to Bentley's layers. This "Bentley length" L_B varies from about 0.8 m, when the air surrounding the crystal is near −15°C, to 8 m near −19°C, both of which are much less than the estimated crystal fall-paths of ∼1800–2000 m for these temperatures. Thus, crystals should pass through enough regions to account for the variety. Of the three sources, the heterogeneities produced the most variety. The total value depends on the assumed resolution, but for micron-scale resolution, the variety is $\sim 10^{500}$, which is much less than previous estimates, though still immense. The results apply only to single crystals grown in relatively ideal conditions (yielding the more picturesque forms), but the model may be extended to irregular forms and more realistic conditions in typical snow clouds.

2 Diversity and growth

2.1 Shape diversity as the logarithm of variety

Regardless of how we estimate it, the variety, or number of possible distinguishable shapes, will be a very large number. For this reason, we instead work with shape diversity S, defined here as the base-10 logarithm of the variety. As such, the diversity is similar to entropy, which is proportional to the logarithm of the number of possible states instead of distinguishable shapes[2]. The shape diversity has similarities and differences with the diversity that we perceive upon viewing snow. For example, both types of diversity will be large when crystals can grow in a wide range of conditions. But the diversity we perceive in some crystal collection will depend on the degree and kind of differences between the crystals, not just on the existence of differences. However, this perceived diversity is hard to define unambiguously, whereas the shape diversity can be analysed mathematically. So, we analyze the latter in the hope that the results shed light on the former.

2.2 Distinguishing shapes

One can characterize a crystal shape by the dark lines in its image, lines that mark places where growth produced a sharp bend in the surface. For our purposes, these lines are the crystal features. For example, the feature of the crystal in Fig. 1a is the perimeter, traced and scaled-down at right. Crystals in Fig. 1b and c have additional features in the interior, whereas crystals in Fig. 1d and e have more complex perimeter and interior features. Though it may help to picture the crystals from the viewpoint in Fig. 1, such a viewpoint is unnecessary for the analyses that follow. Moreover, even though "feature" is a crucial concept, a precise definition is not needed because we focus on growth-induced feature changes. These changes should be discernable in the following sense. If we resolve lines in the image to resolution *res*, then any change in a section of line (including line splitting) by at least *res* would be a distinguishable change. Thus, if two crystals follow paths that are identical, except that one experiences a change in conditions that produces a distinguishable feature change, then the two crystals would have distinguishable shapes.

2.3 Feature changes on single-crystal tabular forms

In this paper, we treat only the growth of single-crystal tabular forms between ∼−9 and −22°C. In this temperature range, the prism-face growth rate is faster than that of the basal. This fact permits a major simplification – the assumption that most features arise from growth of the outermost prism faces. That the growth of these faces

[2]This similarity could be developed two ways: as part of a shape "thermodynamics" or by linking the diversity to the entropy of the crystal and cloud environment. Neither idea is developed here.

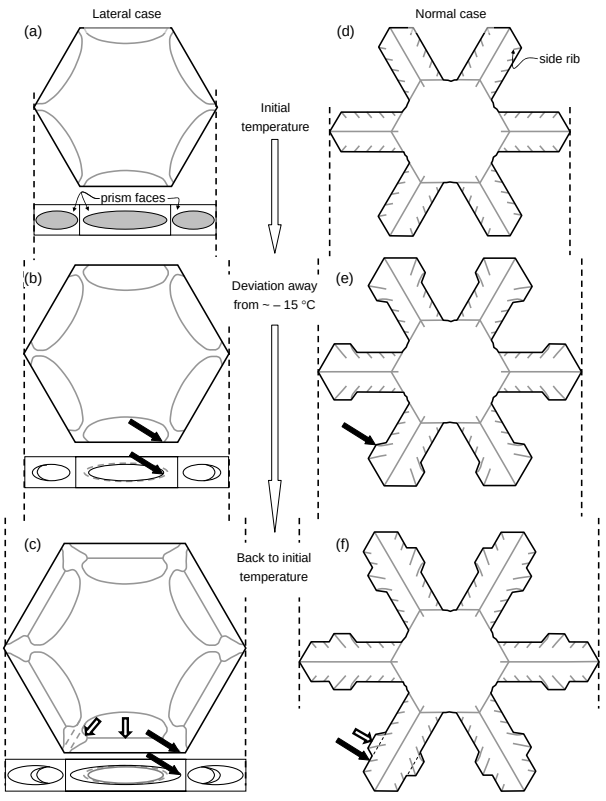

Fig. 2. Two examples of crystal feature changes from temperature changes in a cloud at liquid-water saturation. Left column (top to bottom) shows a feature change on a hollow plate due to growth lateral to the prism axes. **(a)** is the initial crystal. Front view below the sketch shows the pits in the three prism faces. In **(b)**, growth slows as T moves away from the growth-rate peak near $-15°$C, narrowing the lip of the pit (filled arrow). In **(c)**, growth resumes at the faster rate as T returns to its previous value, thus widening the lip of the pit (filled arrow). Grey lines are feature changes due to the growth-rate change, here boundaries of the pits and ribs (hollow arrows). Right column shows a feature change on a stellar crystal due to growth normal to the prism axes. **(d)** is the form from growth under constant conditions. Side ribs and the longer main ribs are ridges on the branch underside (Nelson, 2005). Growth slows in **(e)**, as T moves away from the growth-rate peak, widening the tip (solid arrow), before resuming at the faster rate, at the previous T, and narrowing in **(f)** (solid arrow). Hollow arrows mark the feature changes in both cases. If growth had not slowed, the features would instead follow the dashed lines.

controls the perimeter of a simple, solid hexagonal plate (e.g. Fig. 1a) needs no explanation. But the growth history of these faces should determine other feature changes too. For example, in the case of a hollow plate (Fig. 2a–c), when the prism-face growth temporarily slows, the hollows can decrease in size, producing a wiggle in an "interior" line and the splitting of the perimeter line shown in the figure. For the case of a stellar crystal, a similar growth-rate change can produce a 'band' on each branch (Fig. 2d–f). A recent study of various

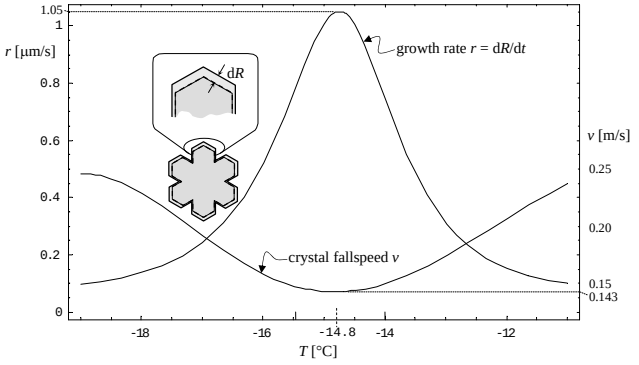

Fig. 3. Prism-face growth rates (left axis) and fallspeeds (right axis) for crystals grown at constant temperature. Curves are fits to Takahashi et al.'s (1991) data for crystals grown for 10 min. At later times, v increases, most rapidly at temperatures away from the peak, and r decreases slightly, mainly at temperatures away from the peak. (Functional forms are in Appendix C.) Marks on the abscissa mark peaks in r' and r. The basal-face growth rate (not shown) has a minimum where the prism-face has a maximum.

observations suggested how other common features likely arise from prism-face growth-rate changes (Nelson, 2005).

2.4 Prism-face growth changes from temperature changes

The prism-face growth rate r generally depends on crystal size and shape, air pressure, vapor pressure, and temperature. However, sufficiently extensive data are available only for constant-temperature measurements of growth under conditions of atmospheric pressure and a vapor pressure equal to equilibrium over pure liquid water. Luckily, these are typical conditions in snow-producing clouds. Snow-producing clouds often contain significant liquid water over much of their lifetime. In such mixed-phase conditions, measurements (Korolev and Isaac, 2006; Siebert et al., 2003)[3] and theory (Shaw, 2000) suggest that the vapor pressure stays near liquid-water saturation. Hence, we will assume that the ambient vapor pressure is at the temperature-dependent liquid-water saturation value. This will greatly simplify the treatment, but we should remember that the results will only apply to such liquid-rich conditions. Moreover, we will ignore crystal-crystal collisions and effects from the close passage of, and collisions with, droplets. Finally, as no measurements of polycrystal growth rates are available, the model is restricted to single crystals. With these assumptions, the air temperature T controls r. This rate has a peak near $-14.8°$C (Fig. 3), which suggests

[3]In the former, measurements were averaged over 100 m. In the latter, air temperature and liquid water content at 15-cm resolution were correlated as if the droplets grew or evaporated to stay near equilibrium.

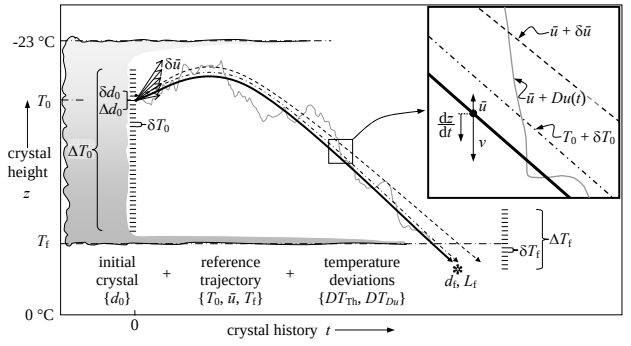

Fig. 4. Overview of growth-deviation model. In a trajectory $z(t)$, a crystal nucleates with diameter d_0 at T_0 in an updraft $\bar{u}$ then falls at speed $v-\bar{u}$ until reaching cloudbase at temperature T_f (solid curve). Each resolvable variation δd_0, δT_0, $\delta\bar{u}$, and δT_f results in a final diameter d_f that changes by $\pm 2 \bullet res$ (dashed curves). Variable ranges are Δd_0, ΔT_0, $\Delta\bar{u}$, and ΔT_f, making the number of distinct reference classes $N_0 \bullet N_{\rm ref} = (\Delta d_0/\delta d_0) \bullet (\Delta T_0/\delta T_0 \Delta\bar{u}/\delta\bar{u} \Delta T_f/\delta T_f)$. Values are in Table 1. DT_{Th} and DT_{Du} (from updraft deviations Du – dotted curve) are temperature deviations that further alter crystal shape. For each trajectory, the number $N_{\rm dev}$ of deviation-caused shape changes depends on d_f/res, the final pathlength L_f, and the number of relevant deviations/meter ($F_{Th}+F_{Du}$).

that we must carefully track the temperature to estimate when distinguishable changes to growth features can occur.

3 Crystal trajectories and diversity sources

With r depending only on T, the initial crystal properties and temperature history determine the final crystal form. We now study these influences in detail.

3.1 Initial crystals and reference trajectories

Most snow crystals start as frozen droplets. Subsequent growth may be affected by various crystalline imperfections from the freezing process, but the effects are poorly understood[4]. So, we characterize the initial crystal by its diameter d_0. The initial temperature T_0 is also an initial characteristic, but we instead use T_0 as a trajectory parameter.

Temperature changes along a crystal trajectory are due to spatial air-temperature heterogeneity DT_{Th}, which exists at a fixed time, and the altitude-dependent air temperature in the absence of temperature heterogeneity, which occurs during the crystal's up-down motion. The latter is the sum of that from 1) slowly varying altitudes for a crystal in an updraft of constant speed, and 2) heterogeneity DT_{Du} from altitude deviations due to updraft-speed deviations Du. Horizontal motion is ignored.

[4]Under slow growth conditions, dislocation outcrops on the surface influence growth. During freezing, chemical impurities may lead to dislocations or produce other surface effects. Also, larger drops are more likely to freeze with internal stresses and become polycrystals, particularly at low temperatures.

Table 1. Trajectory results for d_f, L_f, S_0, and $S_{\rm ref}$.

T_0[°C]	−11	−13	−15	−17	−19
$d_f^{\rm a}$ [μm]	441	1843	7600	3919	2069
$L_f^{\rm a}$ [m]	686	1227	1850	1866	2009
$\delta d_0^{\rm a}$ [10^{-7}m]	96	52	38	2.9	3.2
$\delta T_0^{\rm a}$ [10^{-3} °C]	9.1	1.4	1.5	1.2	4.4
$\delta\bar{u}^{\rm a}$ [10^{-5} m/s]	110	27	5	25	100
$\delta T_f^{\rm a}$ [10^{-2} °C]	4.3	2.8	2.2	5.1	10
$S_0^{\rm b}$	0.7	1.0	1.2	1.5	1.5
$S_{\rm ref}^{\rm b}$	7.5	9.3	10.1	9.1	7.5

[a] Baseline case (1 below), res=1 μm. (cloud is 2143-m thick).
[b] Average of cases 1–4: {d_0 [μm], $\bar{u}$ [m/s], T_f [°C]}=1: {8, 0.12, −8}; 2: {1, 0.12, −8}; 3: {1,0.01, T_0+1}; 4: {40, 0.25, T_0+11}.

To account for these temperature deviations, we write the crystal temperature at time t as $T(t)=T(z(t))+DT(t)$, where $T(z(t))$ is the temperature for a crystal lofted in an updraft with the cloud-averaged speed $\bar{u}$, in which the altitude is $z(t)$, and $DT(t)$ is the total temperature deviation along a trajectory ($=DT_{Th}+DT_{Du}$). A given trajectory $z(t)$, hereafter a "reference" trajectory, changes as $dz/dt=\bar{u}-v$, where v is the crystal's terminal fallspeed and $T(z)$ decreases with z as $dT(z)/dz \equiv T' = -7\times10^{-3}$ °C/m, a typical environmental lapse rate. An actual updraft has speed $\bar{u}+Du(t)$, but Du is used only to estimate DT_{Du}, not for calculating trajectories. These and other model parameters are sketched in Fig. 4 and a full listing of symbol definitions is in Appendix A.

The duration of a trajectory depends on T_0, T_f, $\bar{u}$, and how quickly v increases. The fallspeed depends on crystal shape, and increases slowest for the crystals that grow the fastest (Fig. 3). These crystals fall slowest because, as tabular crystals fall broadside to the airflow, the broadest (and thinnest) crystals expose the greatest area to the airflow, and thus have the greatest drag force. Hence, the crystals that grow the fastest also fall the slowest, and end up with the longest growth times.

3.2 Three sources of diversity

A reference trajectory begins when a crystal nucleates at temperature T_0 from a droplet of diameter d_0. Here $-11 \geq T_0 \geq -19$°C. Typically, $\bar{u}$ exceeds the fallspeed of the micron-sized frozen droplets, so the crystal initially rises and thus cools.

When v reaches $\bar{u}$, the crystal has its maximum altitude[5] and minimum T, and thereafter falls towards cloudbase at the warmer temperature T_f where growth is assumed to stop. (Growth below cloudbase is ignored, even though the vapor pressure exceeds ice saturation for some distance.) The temperature deviations then superimpose on the reference trajectories. During such a history, the origin of crystal variety can be divided into three sources: variations in the initial diameter, variations in the reference trajectory, and temperature deviations due to cloud heterogeneities. From these varieties, the corresponding diversities are calculated.

Each source is treated separately. Let N_0 be the number of possible forms due to variations of the initial crystal diameter, a number that will generally depend on the reference trajectory. Similarly, $N_{\rm ref}$ is the corresponding number for the reference trajectories, and may depend on the initial diameter, whereas $N_{\rm dev}$ is the corresponding number for deviations. $N_{\rm dev}$ will generally depend on the initial crystal size and trajectory parameters. The shape diversities from these influences

$$\begin{aligned} S_0 &= \log_{10}[N_0], \\ S_{\rm ref} &= \log_{10}[N_{\rm ref}], \qquad \text{and} \\ S_{\rm dev} &= \log_{10}[N_{\rm dev}], \end{aligned} \tag{1}$$

are evaluated next.

4 Variations of initial crystal and reference trajectories

To evaluate S_0, $S_{\rm ref}$, and $S_{\rm dev}$, we use the numerical integration method in Appendix B to track the crystal diameter $d(t)$, temperature $T(t)$, and pathlength $L(t)$ (air depth the crystal falls through) for time t along reference trajectories. First, we use the reference trajectories to analyze S_0 and $S_{\rm ref}$. A trajectory is determined by d_0, T_0, T_f, $\bar{u}$, and v. But v depends on d_0 and $T(t)$ through the crystal size and shape. Thus, reference trajectories depend only on d_0, T_0, $\bar{u}$, and T_f. Upon exiting cloudbase, the crystal has diameter d_f and total pathlength L_f.

4.1 Distinguishable reference classes for trajectories without deviations

Consider a reference trajectory with some values of d_0, T_0, $\bar{u}$, and T_f, but one variable, say $\bar{u}$, is varied by $d\bar{u}$. For all $|d\bar{u}|$ less than some value, defined as $\delta\bar{u}$, the final crystal forms will be indistinguishable. (Ignore cloud heterogeneities for now.) When $|d\bar{u}|>\delta\bar{u}$, the resulting crystal will have some feature displaced by at least *res* from that on the original ($|d\bar{u}|$=0) crystal. To determine δd_0, δT_0, $\delta\bar{u}$, and δT_f, we consider changes to d_f, a common feature that is relatively sensitive to the temperature history. Thus, if variable X with value x results in d_f, then value $x+\delta X$ results in $d_f \pm 2\bullet res$. So, if d_f is sensitive to X, then δX will be relatively small. Crystals within $d_0\pm\delta d_0/2$, $T_0\pm\delta T_0/2$, $\bar{u}\pm\delta\bar{u}/2$, and $T_f\pm\delta T_f/2$ are said to be in the same "reference" class; they can have complex features, yet would be observed as indistinguishable.

[5]For updrafts considered here, the altitude increase is typically less than 100 m.

4.2 Number of reference classes

To estimate S_0 and $S_{\rm ref}$, we need a typical range of each variable. Call these Δd_0, ΔT_0, $\Delta\bar{u}$, and ΔT_f. The resulting number of possible distinguishable crystals due to changes in d_0 is N_0=$\Delta d_0/\delta d_0$, though this number will depend somewhat on the values of d_0, T_0, $\bar{u}$, and T_f used to calculate δd_0. The corresponding numbers for the other variables are $\Delta T_0/\delta T_0$, $\Delta\bar{u}/\delta\bar{u}$, and $\Delta T_f/\delta T_f$. We assume that d_0 varies between 1 and 40 μm, T_0 varies between -10 and -20°C, $\bar{u}$ varies between 0.01 and 0.25 m/s, and T_f (always $>T_0$) varies between -9 and -17°C. Thus $\{\Delta d_0, \Delta T_0, \Delta\bar{u}, \Delta T_f\}$=$\{39\,\mu$m, 10°C, 0.24 m/s, 8°C$\}$.

Use of the calculated trajectories showed that the diversities S_0 and $S_{\rm ref}$ depended on d_0, T_0, $\bar{u}$, and T_f, with the greatest dependence being on T_0. Averaging over the results from five T_0 (Table 1) gives S_0=1.2 and $S_{\rm ref}$=8.7. S_0 is small because d_0 has a significant influence only at the start; for example, a crystal that begins 2-μm larger will end about 2-μm larger. This suggests that $S_0\approx\log_{10}[\Delta d_0/2\bullet res]$=1.3. The value is instead 1.2 because d also affects v. $S_{\rm ref}$ is much larger, mainly because d_f is sensitive to T_0 and $\bar{u}$, both of which affect T (and hence r) throughout the trajectory. In contrast, T_f only affects L_f, thus adding relatively little to $S_{\rm ref}$.

5 Temperature deviations due to cloud heterogeneities

A given reference class represents a certain shape. We do not know this shape, but we nevertheless can consider possible variations to the shape, variations that arise from air-temperature and updraft-speed heterogeneities along the fall-path. As a crystal falls, the heterogeneities produce a continuously varying DT that alter the crystal's growth features. But there will be some average duration between relevant DT changes, that is, between DT changes that can produce distinguishable changes to the crystal features. As there can be many possible sequences of relevant changes, each reference class can contain many possible crystal forms.

After a relevant change, the feature may change further. For example, if a sidebranch sprouts and no further DT deviations occur, subsequent growth is determined by the rest of the trajectory. Otherwise, subsequent relevant DT deviations will affect the shape according to when they occur. To proceed, we first estimate the number of relevant deviations and then consider when each one may occur.

5.1 Number of relevant deviations

We set a growth-amount criterion for the relevant deviations, then estimate how often the criterion is satisfied for a given crystal path. In time dt, a crystal falls through pathlength $dL=v\,dt$ as its outermost prism faces advance by $dR=r\,dt$, where r is the prism-face growth rate (Fig. 3). ($dL\neq dz$ unless $\bar{u}$=0.) A temperature differing by DT_i produces a growth-rate change $dr_i=r'DT_i$, where $r'\equiv dr/dT$ is the growth-rate sensitivity and "i"="Th" or "Du". The size of the surface perturbation thus produced is $d^2R_i=dr_i\,dt$. (For a lateral deviation (e.g. Fig. 2a–c), the growth rate is unknown, so we use r as an approximation.) Integrating d^2R_i between depth L_t at time t and L_t+L at time $t+L/v$ gives δR_i:

$$\delta R_i(L_t, L)=\int_{L_t}^{L_t+L} r'(x)DT_i(x)v^{-1}(x)dx$$
$$\equiv r'v^{-1}\Sigma_i(L_t, L), \quad (2)$$

where the T changes are small enough to remove r'and v from the integrand. The number of relevant deviations in Σ_t is nearly independent of L_t, so we will ignore this dependence. For a surface perturbation to enlarge, it must receive more vapor flux than adjacent regions. To do so, δR must exceed the vapor mean-free path λ, which we fix at 0.08 μm (λ varies only slightly with T and z). Assuming that the perturbation continues to grow, eventually exceeding *res*, the perturbation from Eq. (2) can change a feature when

$$\Sigma_i(L)\geq\frac{\lambda v}{r'}\equiv p. \quad (3)$$

The parameter p greatly influences $S_{\rm dev}$ due to the sensitivity of v and r' to T. During growth, p generally increases due to the increase of v. For crystals with T_0=−15°C, p increases slowly, and much of the growth occurs with $p\sim$0.018°C m. In contrast, crystals with T_0 near −11 and −19°C have faster-rising values of p that average about 10 and 20 times larger.

5.2 Distribution functions from stratus clouds

The number of times that Eq. (3) is satisfied depends on p and L. To handle this dependence, we define peak distribution functions $F_i(p)$ as the number of peaks exceeding p in unit L. To estimate $F_i(p)$, I used data from horizontal flight paths in stratus clouds with T<0°C. The values of DT_{Th} were direct measurements, but DT_{Du} required integration of Du to get the altitude deviation Dz, from which $DT_{Du}=T'Dz$. (The integration introduced factor v^{-1} into δR_{Du}, and thus F_{Du} also depends on v.) Then I integrated DT_i to obtain Σ_i, from which the F_i were derived. Details are in Appendix D.

The F_{Th} functions from two cloud datasets decayed as $p^{-0.66}$ and agreed within a factor of two, even though the clouds had different temperature averages and the measurements were done differently (Fig. 5). In contrast, only one cloud dataset was available for F_{Du}, and the values decayed as $p^{-0.50}$. The reason F_i decay with increasing p is because larger temperature deviations are rarer, but the reason for exponents −2/3 and −1/2 is unclear.

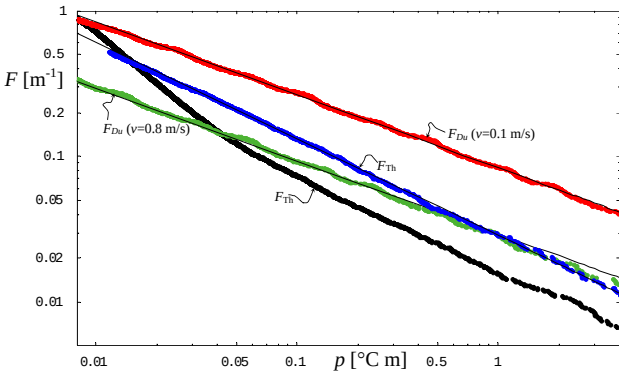

Fig. 5. Temperature deviation distribution functions F_{Th} and F_{Du}. All functions are from measurements at 15-cm intervals except the lower F_{Th} one, which instead had 8-mm intervals. Also shown are fits F_{Th}=0.0287 $p^{-0.66}$ and F_{Du}=0.0262 $p^{-0.50}v^{-0.5}$.

The reciprocal of the sum of the distribution functions is the fallpath needed for a feature to form. This distance is analogous to the layer thickness mentioned by Bentley (even though "layer" suggests homogenous, horizontally extended regions, neither of which may occur). To acknowledge his insight, let us call this the Bentley length L_B:

$$L_B(p, v)\equiv\frac{1}{F_{Th}(p)+F_{Du}(p, v)}. \quad (4)$$

Using the estimated minimum p of 0.018 with v=0.1 m/s, which applies to a small crystal growing near −14.8°C, the total value of F is ∼1.2 m^{-1}, making $L_B\sim$0.8 m. In contrast, a maximum p of 0.36 with v=0.4 m/s (appropriate for a large crystal near −19°C) gives $L_B\sim$8 m. Most values of L_B should lie in between these extremes.

5.3 Number and positions of feature changes

For constant p and v, the number of times n that a temperature deviation can change a feature is the ratio of the total pathlength with the Bentley length. But only some fraction χ of the deviations will grow into a distinguishable feature change, so

$$n=\frac{\chi L_f}{L_B(p, v)}. \quad (5)$$

Each of these feature changes could have been born when the outermost prism faces were at any one of m distinct radial positions on the crystal. As these will be separated by intervals of *res*, we have

$$m=\frac{d_f}{2\cdot res}. \quad (6)$$

Table 2. Combinatorial parameters n and m for $S_{\rm dev}$.

T_0 [°C]	−11	−13	−15	−17	−19
n[a]	48.8	229.9	467.5	213.0	88.6
m[b]	220.6	921.3	3799.9	1959.7	1034.3
$\log_{10}[2me/n]$	1.4	1.3	1.6	1.7	1.8

[a] Based on L_f from Table 1, and the average $F_{Th}+F_{Du}$ for the coldest and warmest parts of the trajectory.
[b] $m=d_f/2res$, with d_f from Table 1.

That is, there are m resolvable growth intervals. m and n are used below to calculate $S_{\rm dev}$. Although m depends on both the resolution and trajectory (through d_f), n depends only on the trajectory.

5.4 Estimates of L_f, d_f, m, and n

The reference trajectories were used to estimate L_f and d_f (Table 1), and then m and n. The values of L_f increased as T_0 decreased because the distance to cloudbase increased, but the increase is most rapid as T_0 approaches −15°C from lower heights due to the decrease in v (Fig. 3). The value of L_f could greatly exceed the cloud thickness when $\bar{u}$ was large (≥0.25 m/s) and T_0 was near −15°C (where v was small), but even at other values of $\bar{u}$ and T_0, the value greatly exceeded L_B. Like L_f, the diameter d_f initially increases as T_0 decreases, but in contrast, d_f decreases above −15°C. This peak is due to both the maximum in r and the minimum in v. From Eq. 6, m has an analogous peak. The n maximum near −15°C (Table 2) also has two causes: the trend in L_f and the peaks in r' at −14.0 and −15.4°C (Fig. 3) that greatly decrease L_B. In Sect. 6.2 below, we integrate $dn=dL\chi/L_B(p,v)$ for more precise analysis and show that a double-peak exists.

5.5 Combinatorial method for $S_{\rm dev}$

Within a reference class, a crystal has n feature changes that can arise in m growth intervals, each of which may be born during either a growth spurt or lull, meaning that each interval can develop one of two possible feature changes[6]. The resulting number of feature-change combinations is an application of a common calculation (Feller, 1968):

$$N_{\rm dev}=\binom{m}{n}2^n=\frac{m!}{n!(m-n)!}2^n. \quad (7)$$

[6]Only $m\geq n$ makes sense, so n must be limited to m. If *res* exceeds about 5 μm, $n>m$ for some conditions and the analysis becomes more involved, though one could argue that the RHS of Eq. 7 becomes 2^n.

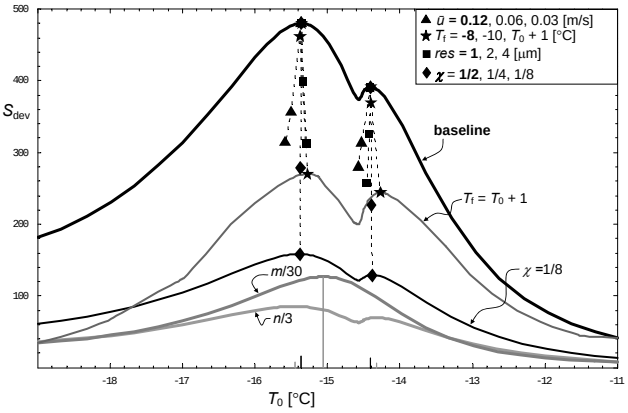

Fig. 6. Shape diversity $S_{\rm dev}$. The upper black curve, the baseline case (bold values in legend), is derived from the grey curves of m (reduced 30-fold) and n (reduced 3-fold). Solid triangles, stars, squares, and diamonds mark peak positions for other values of $\bar{u}$, T_f, χ, or res. Full curves show cases χ=1/8 and $T_f=T_0$+1. Vertical lines on the abscissa are peak positions and relative magnitudes for the baseline case (black lines), the value of m (long grey line), and the value of n (short grey lines).

As $m\gg1$, $n\gg1$, and $m-n\gg1$ (Table 2), Stirling's factorial approximation can be used:

$$N_{\rm dev}\approx\frac{2^n}{\sqrt{2\pi n(1-\frac{n}{m})}}\frac{(\frac{m}{n}-1)^n}{(1-\frac{n}{m})^m}. \quad (8)$$

When $m\gg n$, $N_{\rm dev}$ approaches $(2\pi n)^{-1/2}(2me/n)^n$, showing that $N_{\rm dev}$ increases rapidly when either m or n increase. In this case

$$S_{\rm dev}\approx n\cdot\log_{10}[\frac{2m\cdot e}{n}]-\frac{1}{2}\log_{10}[2\pi n]. \quad (9)$$

When $res<4\,\mu$m, Eq. (9) is accurate to within 1–3% of the value derived from Eq. (7).

6 Discussion

6.1 Cloud heterogeneities as the main source of diversity

As $\log_{10}[2me/n]>1$ and $n\gg1/2$ (Table 2), Eq. (9) suggests that $S_{\rm dev}$ exceeds n, which exceeds $S_0+S_{\rm ref}$ for all T_0. Further analysis of the dependence of S_0, $S_{\rm ref}$, and $S_{\rm dev}$ on *res* showed that this finding is independent of viewing resolution, provided that *res* was not so large that $m<n$. Hence, of the three sources, air-temperature and updraft heterogeneities dominate the diversity. So, we examine this source further.

6.2 Further examination of $S_{\rm dev}$: the "mitten" curve

A plot of $S_{\rm dev}$ versus T_0 reveals a curve in a mitten-like shape (Fig. 6). Specifically, for most cases considered, the curve has a larger, broader peak near -15.4°C and a smaller, narrower peak near -14.4°C. The two peaks come from n, which is double-peaked because r' has maxima on both sides of the growth-rate peak near -14.8°C. The lower-temperature peak of $S_{\rm dev}$ is larger partly because only lower-temperature crystals experience both r' maxima during their descent. In addition, crystals that start at lower temperatures have greater $S_{\rm dev}$ due to their larger d_f, which is partly due to their longer L_f. These asymmetries are greatly reduced when the cloudbase is only 1°C warmer than T_0, making the curve more nearly symmetric about the growth rate peak.

To better understand the T_0 dependence, consider how the crystal-growth properties r, r', and v affect $S_{\rm dev}$. In the baseline case, $S_{\rm dev}$ changes from 41.3 at -11.0°C to 479.9 near -15.4°C, an increase of 438.6. But when the $T_0 = -11$°C case was run with $r(T)$ evaluated 4.4°C lower (to equal that of a -15.4°C crystal), the resulting $S_{\rm dev}$ was 64.0, an increase of 22.7. If instead v was evaluated 4.4°C lower, the value of $S_{\rm dev}$ increased by 33.4. However, when r' was evaluated 4.4°C lower, $S_{\rm dev}$ increased by 60.2, the largest increase[7]. Therefore, v had a larger effect on $S_{\rm dev}$ than r, but r' had the largest effect.

In nature, the biggest crystals are usually observed to be the most elaborate. This observation can be explained as a combination of two factors. One, $S_{\rm dev}$ increases with the factor m, which is largest for the largest crystals (Eq. 9). Two, the peaks in $S_{\rm dev}$ are mainly due to the nearby peaks in r' and the minimum in v, both of which are either close to or at the maximum in r, and these conditions (large r, small v) are exactly the conditions that produce the largest crystals. Therefore, large crystals form under nearly the same conditions that are needed for maximum diversity.

6.3 Sensitivity and uncertainty in $S_{\rm dev}$

$S_{\rm dev}$ was relatively insensitive to T_f but sensitive to $\bar{u}$. A decrease in T_f decreased $S_{\rm dev}$ for all crystals, particularly those that started near cloudbase. But the decrease is relatively small, and peak temperatures shifted only slightly to higher T_0 (Fig. 6, stars). The latter occurred because a raising of cloudbase decreases L_f. A greater decrease in $S_{\rm dev}$ occurred when $\bar{u}$ decreased to 0.03 m/s. In this case, the peak temperatures shifted to lower T_0. The lower values are due to the shorter L_f, and the decrease in peak temperatures occur because T_0 must decrease to have the same minimum temperature, where much of the growth occurs.

[7]The sum of the individual effects is 116.3, much less than the curve's 438.6. This difference is because $S_{\rm dev}$ depends nonlinearly on r, r', and v. When all three parameters were 4.4°C lower, $S_{\rm dev}$ increased by 366.1. The remaining difference is because the -11.0°C case is closer to cloudbase.

In contrast, $S_{\rm dev}$ was sensitive to *res* and χ. If the resolution is coarser, then *res* is larger and the diversity is less. For example, Fig. 6 shows that the peak diversity decreases by about 170 when *res* increases from 1 to 4 μm. This decrease is due to a decrease in m. Even greater sensitivity comes from χ due to the proportionality of n to χ. For example, when χ decreased from 1/2 to 1/8, the peak diversity decreased from 486 to 160. The value χ=0.5 used in the baseline case is uncertain and likely depends on crystal form, feature type, and the size and rate of the deviation. Qualitatively, χ should be relatively large near peak growth rates, due to the step-clumping that leads to various feature changes (Nelson, 2005), yet may be nearly zero for small, slow-growing crystals that have not yet hollowed (e.g. Fig. 1a). So, χ=0.5 may overestimate $S_{\rm dev}$, at least at slow growth rates, though its functional form and numerical value remain highly uncertain. When χ becomes better known, it can be inserted into the present model.

6.4 Neglected influences on diversity

The vapor pressure in a cloud cannot always be exactly at liquid-water saturation. For example, in a updraft, a region devoid of droplets will be slightly supersaturated (Shaw, 2000), whereas a similar region in a downdraft will be undersaturated. Also, entrainment of subsaturated air can create subsaturated regions. Moreover, if nearly all of the droplets freeze, the vapor pressure can decrease to near ice saturation. Unfortunately, we have no fine-scale data on vapor-pressure deviations from liquid-water saturation. When such data become available, we could use the same method as that used here for T. In particular, Eqs. (2) and (3) would apply, with the necessary substitutions, giving rise to a third distribution function that would appear as a third term in the denominator of Eq. (4). As a result, L_B would decrease and n would increase, thus increasing $S_{\rm dev}$. However, unlike T, vapor-pressure has no altitude term, which is large in the temperature case: $F_{Du} > F_{Th}$ for a range of v (see Fig. 5). The lack of an altitude term would reduce their contribution, though vapor-pressure heterogeneities may still add much diversity.

Other potentially major sources of variety are the initial crystal's structure and close passages/collisions of droplets. When the growth rate is low, step-producing defects can greatly affect the growth rate of a prism face (Wood et al., 2001). Moreover, crystals nucleated under different conditions can end up with different shapes (Yamashita, 1973). But we have little knowledge of either influence. Also, droplets may pass close to, and land on, a crystal, thus locally changing the humidity and temperature. For example, the droplet density can affect the growth rate (Takahashi and Endoh, 2000; Castellano et al., 2007) and cause clear feature changes in some cases (Hallett and Knight, 1994), though quantitative treatment is not presently possible.

Finally, we consider the role of basal-face growth on feature changes. According to our analysis of the mitten curve,

diversity is most sensitive to the growth-rate sensitivity r'. But for the temperature range considered here, the basal face growth rate is relatively insensitive to temperature. For example, between about -11 and -15°C, the basal-face growth rate changes by only about $0.025\,\mu$m/s, much less than the corresponding $0.9\,\mu$m/s of the prism-face (Takahashi et al., 1991). The sensitivities of the two faces are more nearly the same near the tabular-columnar transition temperatures (near -9 and -23°C), but feature changes are relatively rare at such temperatures. At other temperatures, the basal face might have relatively little direct influence on the diversity.

6.5 Errors from using non-ideal datasets

Model results are based on the available data, which, unfortunately, are not perfectly suited for applications to real crystal trajectories in snow clouds. Three problems are mentioned here. One, although crystals fall vertically through the air currents, the only available data on temperature and updraft heterogeneity are from measurements along near-horizontal flight paths. If, for example, the temperature deviations along a vertical path are more spread out than they are along the horizontal and the distribution function has the same power-law scaling, then one can show that the distribution functions would be smaller. Two, snow clouds can have regions with values of $\bar{u}$ much larger than the values here (Wolde and Vali, 2001). However, larger values of $\bar{u}$ would produce unrealistically large crystals, so the baseline-case $\bar{u}$ here may be a reasonable average. Three, data on r and v cover only idealized, constant conditions, and even in these conditions are imprecisely known. For example, more recent, yet limited, data suggest that the growth-rate peak is flatter on top than that shown in Fig. 3 (Takahashi et al., 2008). However, such a change would not alter the main findings here. Finally, in an actual cloud, side-to-side (leaf-like) falling motion and changing temperatures may alter r and v. These considerations show that new measurements of cloud and snow-crystal growth properties are needed to advance our modelling of snow-crystal diversity.

6.6 The total diversity

Because all three sources of diversity, particularly $S_{\rm dev}$, vary with the crystal-cloud variables, the total diversity $S_{\rm tot}$ is not a simple sum of S_0, $S_{\rm ref}$, and $S_{\rm dev}$. Rather, an accurate estimate of $S_{\rm tot}$ would involve calculating the logarithm of a sum of $N_{\rm dev}$ over the reference classes. Instead of attempting such a sum, we estimate an upper limit to S as the sum of the maximum values of S_0, $S_{\rm ref}$, and $S_{\rm dev}$. For χ=½ and res=1 μm (a relatively high optical-microscope resolution), this upper limit is 1.5+10.1+475≈487. Given the various uncertainties involved and neglected influences on diversity, the actual number may be larger by several orders of magnitude. Nevertheless, unless χ exceeds ½ near -15°C, then an upper limit to the total diversity $S_{\rm tot}$ should be about 500.

6.7 Comparison to previous estimates

The upper limit $S_{\rm tot}\sim$500 is large, yet much less than previous estimates. Knight and Knight (1973) estimated the number of molecules in a typical snow crystal and then considered, but did not evaluate, the number of ways these molecules could be arranged. A lower bound of this number is derived from Eq. (6) by substituting for m a crystal radius divided by the water-molecule diameter and summing over all n (0 to m). The result is 3^m, which, for a radius of 3 mm, gives $S_{\rm tot}\sim 3\times10^6$. In contrast, Hallett (1984) assumed a resolution 3×10^4 times larger (10 μm), yet calculated $S_{\rm tot}\sim 5\times10^6$. His estimate involved consideration of 10^4 "points" on the crystal, apparently each of which could have grown in one of 20 humidity classes and one of 50 temperature classes. (S_0 was ignored.) Based on these assumptions, the number of possible crystals should instead be $(20\times50)^{10\,000}$, which gives $S_{\rm tot}=3\times10^4$. Regardless of their differences, these previous estimates are vastly larger than the $S_{\rm tot}$ found here, and this is mainly because limitations from the growth process were not included. This huge difference in numbers has implications for the following question.

6.8 Comparison to observations: should every snow crystal look unique?

An observational test of the mitten curve is impractical unless *res* is very large. So instead, we check to see if the numbers are reasonable by estimating the likelihood that all crystals in a collection appear unique.

Consider a large, heavy snowstorm that deposits a liquid-water-equivalent snow depth of 3 cm (∼50 cm of snow) over a land area of 10^4 km^2. In total, this equals $\sim3\times10^{11}$ kg of water, which, if each crystal is 10^{-9} kg, amounts to $\sim3\times10^{20}$ crystals, of which $N_c\sim3\times10^{18}$ may have been reasonably symmetric at cloudbase[8]. This number could be compared to the total variety $\sim10^{S{\rm tot}}$; however, the variety of one reference class can be many orders of magnitude different from another. So we instead consider each reference class separately.

[8]Highly symmetric crystals (at typical viewing resolution) are unlikely. For example, Korolev et al. (1999) found that only ∼3% of the sampled crystals were "pristine". But we could average the features over the twelve 30° sectors, one bisector along the center of each branch. Or, we could consider each sector independently, and find the probability that any two, out of all $12N_c$ of the sectors, are the same.

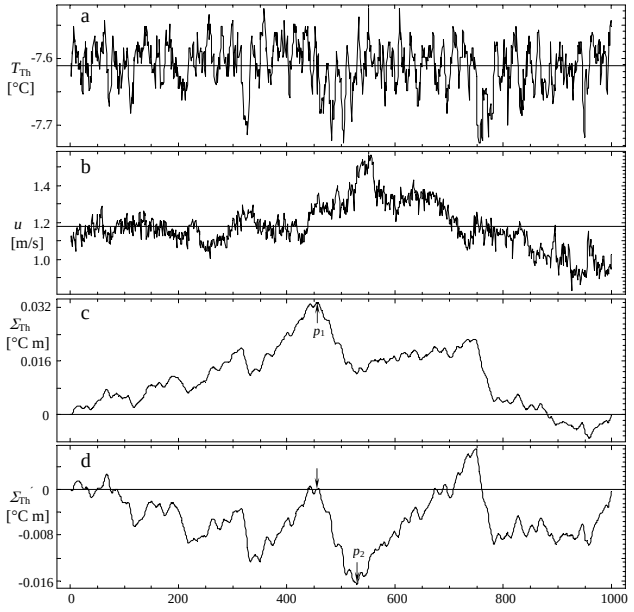

Fig. 7. Analysis of deviations. **(a)** Segment of T_{Th} data. **(b)** Segment of $\bar{u}+Du$ data. **(c)** Integrated temperature Σ_{Th} from section **(a)**. Maximum peak p_1 is marked. **(d)** Σ_{Th} after the peak in **(c)** was removed by breaking the segment into pre-peak and post-peak segments as described in Appendix D. New maximum peak p_2 is marked.

To estimate crystal uniqueness, we assume the crystals are equally likely to be in each class. As a result, the number of crystals per class $N_{\rm ccl}$ is N_c divided by the number of classes, or $N_c/10^{S_0+S\rm ref}$. Using the average S_0 and $S_{\rm ref}$ from Table 1, $N_{\rm ccl}$=4×10^8. (As this exceeds unity, there would be many identical crystals if heterogeneities did not exist.) The probability $pd(i)$ that all crystals in class i are distinct can be estimated by counting the number of ways that this class can have only distinct crystals. This problem is equivalent to the "birthday paradox" problem, which is the surprisingly low probability that all people in a group have birthdays on different days of the year. As $N_{\rm ccl}\gg1$ and $N_{\rm dev}(i)\gg1$, we can use Feller's (1968, end of Sect. 2.3) approximation:

$$pd(i)\approx e^{-\frac{N_{\rm ccl}^2}{2N_{\rm dev}(i)}}. \quad (10)$$

For all crystals to be distinct, each class can have only distinct crystals. Thus, $pd_{\rm all}$, the probability that all crystals are distinct, should be the product of all $pd(i)$. Hence, $pd_{\rm all}<pd(i)$, for all i. Now consider i=0, the class defined as that with the smallest probability. As this class must, according to Eq. (10), have the smallest $N_{\rm dev}$, it requires a warm T_0, a low $\bar{u}$, and a cold T_f; for example, T_0=−11°C, $\bar{u}$=0.02 m/s, and T_f=−10.5°C. Calculation with these numbers gives $N_{\rm dev}\approx5\times10^{16}$, from which $pd(0)$=0.2, suggesting that large snowstorms have enough crystals for some of the smaller crystals to appear as copies.

Table 3. Coefficients for fits to r and v.

value i	a_i	b_i	c_i
1	4.84×10^{-2}	2.04×10^{-3}	0.835
2	0.845	8.00×10^{-3}	2.06×10^{-2}
3	9.88×10^{-2}	0.973	0.866
4	0.613	2.96	1.48×10^{-2}
5	4.56×10^{-2}	2.24×10^{-2}	0.683
6	2.70×10^{-2}	0.788	10.2

Use of a larger *res* or larger sample size would reduce $pd(0)$ even further. As an example of the latter, if we include all snow crystals that have ever fallen on Earth, $N_{\rm ccl}$ increases by many orders of magnitude because $10^{S_0+S\rm ref}$ hardly changes yet N_c increases about 10^{15}-fold (to $\sim10^{33}$; Knight and Knight, 1973). With such a large negative exponent in Eq. (10), $pd(0)$ is negligibly small, meaning that two indistinguishable crystals almost certainly existed. In contrast, for a class $i\neq0$ of crystals with $T_0\sim-15.4$°C, then $pd(i)\approx1$ even if we consider all such crystals that have ever fallen. (Here the exponent is $\sim-10^{-433}$, making $pd(i)=1-10^{-433}$.) So, in this and nearby classes, the crystals should never be the same. Finally, some crystal trajectories are probably more common than others, in which case pd could decrease. Moreover, some crystals may stay close together as they fall and thus experience similar conditions. This too would increase the likelihood of indistinguishable crystals.

The above result is consistent with our experience, but unfortunately is effectively impossible to disprove. For example, even in the first case above where $N_{\rm ccl}\sim10^9$, the number of crystal comparisons is $\sim N_{\rm ccl}^2/2$, which, if each took 1 s, would take a total of $\sim2\times10^{10}$ years. So, even though we may observe all crystals as unique, some of the smaller, relatively compact crystals that were not observed probably include some apparent copies.

6.9 Perceived diversity versus shape diversity

The small crystals that grow near −11 and −19°C contribute little to the total shape diversity, yet seem to add much to the perceived diversity. Specifically, the number of possible forms near −15.4°C is over 400 orders of magnitude greater than that near −11°C. Nevertheless, the small compact crystals, such as those that form near −11 and −19°C, comprise a major portion of snow crystal image collections such as Bentley's (Bentley and Humphrey, 1962), and thus add significantly to our perception of crystal diversity. Why? This is likely because larger differences in form appear more

striking than smaller differences, and the shape diversity does not account for such effects. Nevertheless, the shape diversity is related to the size of the crystal differences in the following sense. Large differences in size are due in part to the growth-rate sensitivity, integrated over a temperature change of a few degrees, and this sensitivity is an important factor in the shape diversity. However, including the degree of crystal-form differences into the analysis would involve adding numerous crystal parameters and subjective factors that may confuse more than clarify the issue.

7 Conclusions

This work presented a systematic way to examine the origin of snow-crystal shape diversity. Some diversity arose from variations in initial crystal size and fall trajectory parameters, though the amounts added relatively little to the total diversity. The main findings involved an analysis of measured in-cloud heterogeneities in updraft speed and air temperature. The number per meter of heterogeneities of size p was found to decay with a power-law exponent of $-1/2$ for updraft speeds and $-2/3$ for temperature. The corresponding Bentley length, the air depth through which a falling crystal can change its features, ranged from 0.8 to 8.0 m. Because such distances are much smaller than typical crystal fallpaths, the heterogeneities can contribute a relatively large amount to the diversity.

Ultimately, the great diversity in snow crystals is due to the extreme temperature sensitivity of the crystal-growth properties that affect the fallpath and Bentley length. For example, one property, the prism-face growth rate, peaks near -15°C, and the effect of this maximum is amplified by the corresponding minimum in fallspeed, resulting in a huge range of crystal sizes. Moreover, shape diversity is strongly influenced by the temperature sensitivity of the growth rate. For crystals originating near – 11°C, the shape diversity is predicted to be low enough that nature produces some apparent copies. But for crystals originating near -15°C, the resulting shape diversity is so high that initially featureless, frozen spheres of ice, falling through updrafts that are heterogeneous yet uniform in appearance, can nevertheless develop into intricate, symmetric crystals that are never the same.

Appendix A

Summary of symbols and terms used in the text

Symbol or term	Definition	1st appears
$d(t)$; d_0; d_f	crystal diameter at time t; initial value; final value	Sects. 3.1 and 4
DT_{Th}; DT_{Du}	temperature deviation by heterogeneity in T; Du	Sect. 3.1
Du	updraft speed deviation	Sect. 3.1
$F_{Th}(p)$; $F_{Du}(p)$	peaks (m^{-1}) in δR exceeding p due to DT_{Th}; DT_{Du}	Sect. 5.2
L; L_f	pathlength crystal falls through air, final value	Sect. 4
L_B	Bentley length scale	Eq. (4)
m	number of distinguishable positions for a feature change	Sect. 5.3
n	number of feature changes in fall path	Sect. 5.3
N_0, $N_{\rm ref}$, $N_{\rm dev}$	number of possible forms from three sources	Sect. 3.2
N_c; $N_{\rm ccl}$	number of crystals; crystals/reference class	Sect. 6.8
p	peak parameter	Eq. (3)
$pd(i)$; $pd_{\rm all}$	probability crystals in class i are distinct; for all classes	Sect. 6.8
r	prism-face growth rate	Sect. 5.1
r'	growth rate sensitivity=dr/dT	Sect. 5.1
R	position of outermost prism face	Sect. 5.1
reference trajectory	crystal path from T_0 to T_f at constant $\bar{u}$	Sect. 3.1
reference class	range of d_0, T_0, $\bar{u}$, T_f, within which all crystals in an ideal trajectory are indistinguishable to *res*	Sect. 4.1
relevant	produces a distinguishable feature change	Sect. 5
res	resolution for distinguishing crystal features	Sect. 2.2
S_0, $S_{\rm ref}$, $S_{\rm dev}$; $S_{\rm tot}$	diversity from threesources; total diversity	Sects. 3.2 and 6.6
$T(t)$; T_0; T_f	crystal temperature at time t; initial value; final value	Sects. 3.1 and 3.2
T'	environmental lapse rate: -7×10^{-3} °C/m	Sect. 3.1
$\bar{u}$	cloud-averaged updraft speed	Sect. 3.1
v	crystal terminal fallspeed	Sect. 3.1
$z(t)$	crystal altitude at time t	Sect. 3.1
δx	range of variable x (=d_0, T_0, $\bar{u}$, T_f) in a reference class	Sect. 4.1
δR	surface perturbation	Eq. (2)
Δx	environmental range of variable x (=d_0, T_0, $\bar{u}$, T_f)	Sect. 4.2
λ	vapor mean-free path: 0.08 μm	Sect. 5.1
Σ_{Th}; Σ_{Du}	integrated temperature deviation from DT_{Th}; DT_{Du}	Eqs. (2) and (3)
χ	fraction of growth perturbations that change a feature	Sect. 5.3

Appendix B

Numerical integration method for reference trajectories

Height $z(t)$ was calculated by summing $dz=(\bar{u}-v)dt$ for timesteps dt, updating v at each timestep. At z=0, T=0°C so $T=T'z$ at each step. If z reached cloudtop (where $T=-23$°C), then dz=0 until $v>\bar{u}$. Only the T dependence of r was considered because r varies little with d and air pressure. The calculation ended when the crystal reached cloudbase at $T=T_f$. The resulting values of L_f, d_f, and n fluctuated with decreasing amplitude as dt decreased from 4 to 0.1 s, so the final values were weighted averages from the various values of dt with greater weight given to smaller dt.

Values of v are unknown for crystals growing with varying temperature, so I used fits to measured values of $v(T, t)$ as follows. I assumed that v primarily depended on d and the crystal's T_0. Thus, t in $v(T, t)$ was replaced by the time it would have taken the crystal to reach diameter d if it had remained at T_0; that is, $(d-d_0)/r(T_0)$. Also, the temperature was set to T_0. Thus, $v(T, t)\rightarrow v(T_0, (d(t)-d_0)/r(T_0))$.

Appendix C

Equations for r, v

Takahashi et al.'s (1991) data on r and v were fit to the following functions. In units of μm/s, $r(T)=a_1+(a_2-a_3(T-T_m)+a_4(T-T_m)^2-a_5(T-T_m)^3+a_6(T-T_m)^4)^{-1}$, where $T_m=-14.8°$C and values of a_i are in Table 3. In units of m/s,
$v(T,t)=V_1(T,t)\bullet V_2(T)$,
where t is time in minutes and
$V_1(T,t)=b_1+b_2V_3(T)t^{(b3+t(V4(T)-b3)/(t+20))}$,
$V_2(T)=1+0.3e^{-0.6(T+22)}-0.21e^{-0.25(T+18)\wedge 2}$,
$V_3(T)=b_4-b_5T+b_6\cos\left[c_1(T+19)-c_2(T+19)^2\right]$,
$V_4(T)=c_3+c_4T+0.06\cos[c_5(T+c_6)]$,
and b_i and c_i are in Table 3. The sole consideration for the above functional forms was to obtain as good a fit to the data as possible.

Appendix D

Determination of the distribution functions

Temperature values T_{Th-i}, with i labelling the data point, represented measurements at equally spaced points 8-mm apart in a 9.60-km-long dataset and 15-cm apart in a 4.05-km dataset. Figure 7a is a data sample. In a given data interval, values of DT_{Th-i} were obtained by subtracting the average value from T_{Th-i}. To obtain the growth-perturbation curve Σ_{Th}, the values of DT_{Th-i} were linearly interpolated and integrated. For u, the same method was used to obtain $D\bar{u}_i$ and then integrated to obtain Dz_i. Using $DT_{Du-i}=T'Dz_i$ (e.g. Fig. 7b), the DT_{Du} data were integrated to obtain Σ_{Du}.

To extract all relevant peaks from the jagged curves of Σ_{Th} (e.g. Fig. 7c and d), I did the following. If the largest peak (positive or negative) occurred at point x_1 with value p_1, then the original T_{Th-i} data were re-averaged over the two segments of i from 1 to x_1 and x_1 to the last value X. The new values of DT_{Th-i} were used to make a new Σ_{Th}'. As the point x_1 is now an endpoint of both sets, Σ_{Th}' equals 0 at x_1 (e.g. Fig. 7d), eliminating peak p_1. But Σ_{Th}' will contain a new peak. Calling this peak point x_2 with peak value p_2, I again divided the set at this point. Assume that $x_2>x_1$. The original set T_{Th-i} was then averaged over three segments: 1 to x_1, x_1 to x_2, and x_2 to X. This process continued, resulting in peak values p_1, p_2, p_3,..., with the values of p steadily decreasing. The iteration stopped when p was so low that no subsequent peak value could produce a feature ($p\sim 0.01°$C m). The values of p were then used to make the peak distribution. By comparing peak distributions for segments of various lengths X, I found that the peak distribution at a given point p' was proportional to X. Thus, the function was scaled by the distance to give the peak distribution per meter F_{Th}. The same method was used for F_{Du}.

Acknowledgements. Szymon Malinowski and Holger Siebert kindly supplied the temperature and updraft data; Tsuneya Takahashi let me use his crystal images; and Marcia Baker, Dennis Lamb, and Duncan Blanchard made manuscript suggestions.

Edited by: T. Garrett

References

Bentley, W. A.: Twenty years' study of snow crystals, Mon. Weather Rev., 21, 212–214, 1901.

Bentley, W. A. and Humphreys, W. J.: Snow Crystals, Dover Publications, NY, 226 pp., 1962.

Castellano, N. E., Gandi, S., and Ávila, E. E.: A numerical study of the effects of cloud droplets on the diffusional growth of snow crystals, Atmos. Res., 84, 353–361, 2007.

Feller, W.: An Introduction to Probability Theory and its Applications, John Wiley and Sons, NY, 1, 3rd edn., 528 pp., 1968.

Frank, F. C.: Snow crystals, Contemp. Phys., 23, 3–22, 1982.

Hallett, J.: How snow crystals grow, Am. Sci., 72, 582–589, 1984.

Hallett, J. and Knight, C. A.: On the symmetry of snow dendrites, Atmos. Res., 32, 1–11, 1994.

Knight, C. and Knight, N.: Snow crystals, Sci. Am., 228(1), 100–107, 1973.

Korolev, A., Isaac, G. A., and Hallett, J.: Ice particle habits in arctic clouds, Geophys. Res. Lett., 26, 1299–1302, 1999.

Korolev, A. and Isaac, G. A.: Relative Humidity in Liquid, Mixed-Phase, and Ice Clouds, J. Atmos. Sci., 63, 2865–2880, 2006.

Nakaya, U.: Snow Crystals Natural and Artificial, Harvard University Press, Cambridge, 510 pp., 1954.

Nelson, J.: Branch growth and sidebranching in snow crystals, Cryst. Growth Des., 5, 1509–1525, 2005.

Shaw, R. A.: Supersaturation intermittency in turbulent clouds, J. Atmos. Sci., 57, 3452–3456, 2000.

Siebert, H., Wendisch, M., Conrath, T., Teichmann, U., and Heintzenberg, J.: A New Tethered Balloon-Borne Payload for Fine-Scale Observations in the Cloudy Boundary Layer, Bound.-Lay. Meteorol., 106, 461–482, 2003.

Takahashi, T. and Endoh,T.: Experimental studies on the dendritic growth of a snow crystal in a water cloud. Proceedings of 13th International Conference on Clouds and Precipitation, Reno, NV, 677–680, 2000.

Takahashi, T., Fukuta, N., and Hashimoto, T.: Vertical supercooled cloud tunnel studies on the growth of dendritic snow crystals, Proceedings of 15th International Conference on Clouds and Precipitation, Cancun, Mexico, http://convention-center.net/iccp2008/abstracts/Program_on_line/Oral_01/TakahashiTsuneya_extended.pdf, last access: 18 September 2008.

Takahashi, T., Endoh, T., Wakahama, G., and Fukuta, N.: Vapor diffusional growth of free-falling snow crystals between −3 and −23°C, J. Meteorol. Soc. Jpn., 69, 15–30, 1991.

Wolde, M. and Vali, G. J.: Polarimetric Signatures from Ice Crystals Observed at 95 GHz in Winter Clouds, Part II: Frequencies of Occurrence, Atmos. Sci., 58, 842–849, 2001.

Wood, S., Baker, M., and Calhoun, D.: New Model for the Vapor Growth of Hexagonal Ice Crystals in the Atmosphere, J. Geophys. Res., 106, 4845–4870, 2001.

Yamashita, A.: On the trigonal growth of ice crystals, J. Meteorol. Soc. Jpn., 51, 307–317, 1973.

Yamashita, A.: Growth processes of ice crystals and a law which is related to the symmetric growth of plate-like snow crystals, American Meteorological Society, Boston, 136–141, 1976.